Bidirectional Power Flow Control and Hybrid Charging Strategies for Three-Phase PV Power and Energy Storage Systems

Cheng-Yu Tang, *Member, IEEE*, Pon-Tzu Chen, and Jia-He Jheng

***Abstract*—The objective of this article is to propose a photovoltaic (PV) power and energy storage system with bidirectional power flow control and hybrid charging strategies. In order to optimize the battery charging performance, five charging strategies, including the constant-current charging, the pulse-ripple-current charging, the sinusoidal-ripple-current charging, the bidirectional pulse-ripple-current, and the bidirectional sinusoidal-ripple-current charging, are adopted. Traditionally, in order to realize these charging strategies, the PV charger should abandon the maximum power point tracking function to maintain the power flow balance. As a result, the output power of the PV array will be decreased. Therefore, bidirectional power flow control strategies are proposed to achieve the maximum PV power utilization as well as to realize the hybrid charging methods. In addition, with the proposed strategies, the bidirectional charging/discharging capability of the battery is able to achieve the maximum PV power utilization. All the proposed strategies can be realized by the digital signal processor without adding any additional circuit, component, and communication mechanism. Theoretical analysis and control principles will also be revealed. Finally, a 5-kW prototype circuit with both simulation and experimental results demonstrate the performance and feasibility of the proposed strategies.**

***Index Terms*—Bidirectional power flow control, hybrid charging strategies, PV power system.**

I. Introduction

OVER the past few decades, renewable energy generation systems, electric vehicles, advanced consumer electronics, and novel energy-saving technologies have been rapidly developed to deal with the fossil fuel usage and carbon dioxide emission issues [1]–[3]. Because of the clean, sustainable, and low-pollution features, the photovoltaic (PV) energy has been paid high attention [4]–[6]. In order to achieve the maximum PV power utilization, the maximum power point tracking (MPPT) is an essential function for the PV power system. Several MPPT algorithms, such as the perturbation and observation (P&O) method and the incremental conductance (INC) method, have been widely adopted [7]–[9]. Besides, a dc–dc converter with the pulsewidth modulation technique should be connected to the PV array to realize the MPPT.

In addition, the battery module is a necessary component for the energy storage in PV power systems. In order to charge the battery from the PV array, the dc–dc converter should act as a PV charger. In the meantime, to ensure the maximum PV power harvesting, the MPPT is also an essential function for the PV charger. Besides, the battery charging performance can be improved to extend the battery life. Therefore, various kinds of charging technologies have been developed [10]–[13]. Traditionally, the constant-current constant-voltage (CC-CV) charging method is adopted for the battery charger. Because of the simple control and the fast charging features, the CC-CV has become one of the most commonly used charging methods. Unfortunately, the continuous charging current might cause the overheat phenomenon. As a result, the electrode plates might be damaged, whereas the battery life will be shortened [14]–[17].

In order to overcome this issue, the pulse-ripple-current charging (PRC) and the sinusoidal-ripple-current charging (SRC) technologies were developed [18]. For the PRC charging, there will be only positive charging current and zero charging in one pulse charging cycle. The charging current is discontinuous while the period of the positive and zero current charging can be adjusted according to different scenarios. In addition, for the SRC charging, the charging current will be continuous and it is regulated as sinusoidal waveform. With the PRC and SRC, electron ions in the battery are able to be homogeneously distributed by the zero charging current period. In other words, the charging performance can be improved.

Moreover, the Reflex^{TM} concept was developed [19]. The Reflex^{TM} method introduces the negative charging period. The negative charging period can stable the chemical reaction of the battery as well as enhance the uniform distribution of electrolyte concentration [20]. The similar bidirectional charging concept can also be adopted for the SRC charging [21]. In [22] and [23], it has been proved that the aged cells can be revived by adopting the discharging (negative charging current) period. The activation energies of migration through the solid electrolyte interface and intercalation of graphite can be provided by the negative charging period. In other words, the inverse reaction of electrolyte can be realized to prevent impedance formation.

Manuscript received February 9, 2021; revised April 4, 2021; accepted May 19, 2021. Date of publication May 25, 2021; date of current version July 30, 2021. Recommended for publication by Associate Editor A. Yazdani. *(Corresponding author: Cheng-Yu Tang.)*

Cheng-Yu Tang and Jia-He Jheng are with the Renewable Energy and Power Conversion Laboratory (REPC), Department of Electrical Engineering,National Taipei University of Technology, Taipei 10608, Taiwan (e-mail: cytang@ntut.edu.tw; s976519@gmail.com).

Pon-Tzu Chen is with the Silergy Technology Inc., Kaohsiung 23557, Taiwan (e-mail: pontzu1126@gmail.com).

Color versions of one or more figures in this article are available at https://doi.org/10.1109/TPEL.2021.3083366.

Digital Object Identifier 10.1109/TPEL.2021.3083366

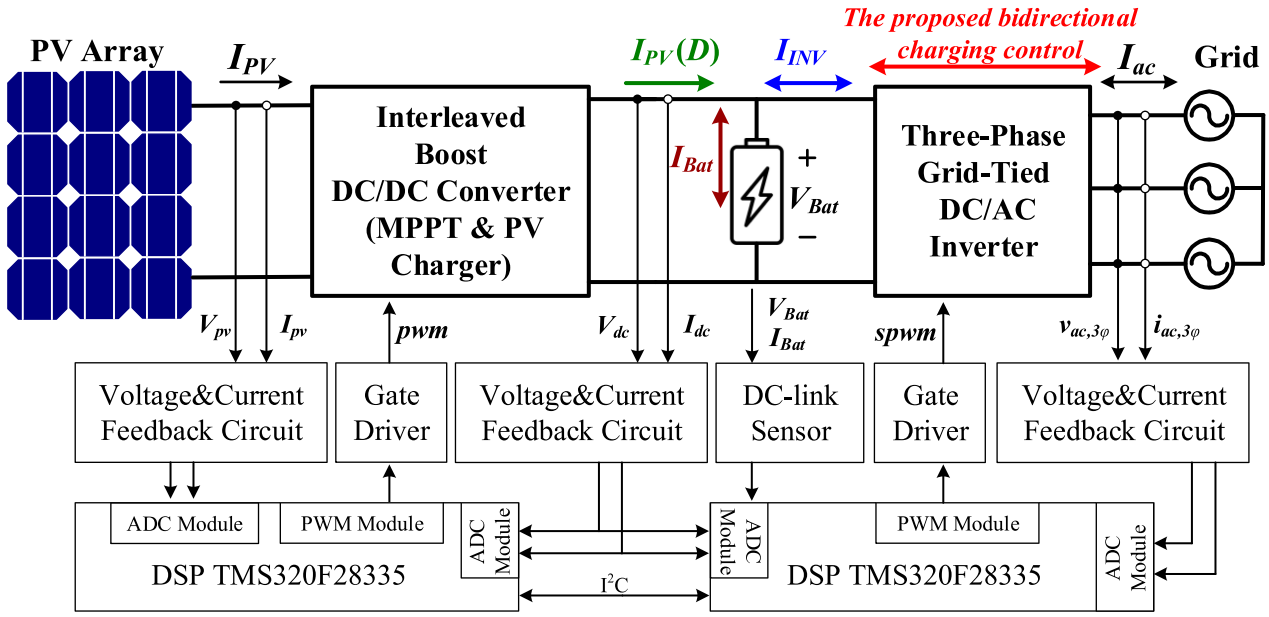

Fig. 1. PV system diagram and control blocks.

Eventually, the battery degradation can be mitigated whereas the state of health of the battery will be improved. Therefore, in our work, the BPRC and BSRC charging are developed according to the advantages of adopting the discharging period.

On the other hand, if the PRC or SRC charging is adopted for the PV charger, the PV power will be regulated as a pulse or sinusoidal waveform, whereas the MPPT function should be abandoned [24]. As a result, the utilization of the PV energy will be reduced. Besides, the bidirectional charging concept is unable to be included for a single-stage PV charger due to the fact that the PV array cannot absorb energy.

Therefore, a three-phase grid-tied inverter integrated with the bidirectional power control capability is proposed in this article. In order to enhance the battery charging performance, hybrid charging strategies are considered and developed. Aims of this article can be summarized as follows: 1) achieve the maximum PV power utilization under different charging methods; 2) realize hybrid charging methods for the battery; and 3) propose bidirectional power flow control strategies for the three-phase grid-tied inverter. Detailed circuit operations, theoretical analysis, and mathematical derivations of the proposed strategies will be presented. Finally, experimental results obtained from a 5-kW prototype circuit verify the performance of the proposed control strategy.

II. PV System Configurations and Basic Charging Concepts

Fig. 1 shows the circuit diagram of the PV power system and control blocks. The two-stage topology is utilized for the PV power system and it is composed of an interleaved boost dc–dc converter, a battery module, and a three-phase grid-tied inverter. The front-end dc–dc converter will be acted as a PV charger. A battery module is included as the dc bus. The rear-end inverter is connected between the battery and the grid to realize the proposed bidirectional charging control. In addition, the digital signal processor (DSP) TMS320F28335 is utilized as the system controller.

Under normal operation, the PV charger should act as an MPPT to harvest the maximum PV power as well as to charge the battery. However, if the required battery charging current is lower than the maximum PV current, the MPPT function will be abandoned, whereas the output PV power and current should be reduced to maintain the power flow balance. As a result, the PV utilization will be decreased, as shown in Fig. 2(a). On the other hand, according to the PV charger proposed in [24], if the PRC or SRC charging method is adopted for the PV charger, the output PV power will be fluctuated between the MPP and the zero power point. Consequently, the system cannot achieve the maximum PV power harvesting due to the power loss area, as shown in Fig. 2(b) and (c), respectively. In addition, because of the single power direction characteristic, the PV panel cannot absorb energy. Therefore, the bidirectional charging and discharging concept mentioned in [25] and [26] is impossible to be realized with a single-stage PV charger.

In view of this, a three-phase grid tie inverter integrated with proposed bidirectional charging control strategies is developed. Detailed operational concepts and theoretical derivations will be revealed in the next section.

III. Proposed Bidirectional Power Flow Control and Hybrid Charging Strategies

In this section, detailed analysis of proposed bidirectional power flow control and hybrid charging strategies will be presented. It is worth mentioning that basic analysis of the three-phase inverter integrated with the CC and PRC charging had

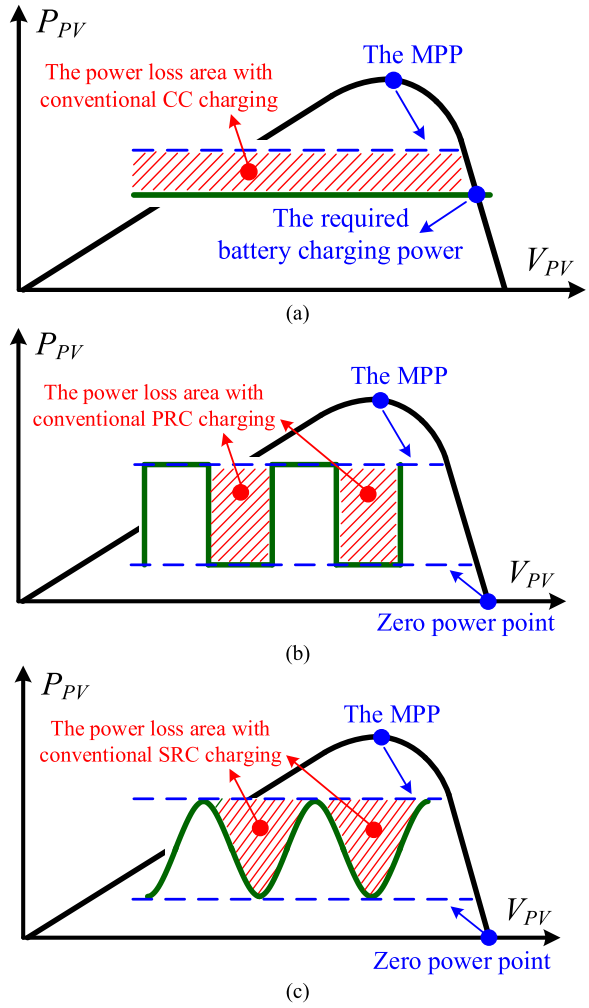

Fig. 2. Conceptual diagram of the power loss area with (a) conventional CC charging, (b) conventional PRC charging, and (c) conventional SRC charging.

been presented in [25] and [26]. However, in [25] and [26], only the single-stage three-phase inverter is adopted, whereas the SRC, BPRC, and BSRC are not proposed. Besides, the detailed charging power analysis of the PV module, the battery, and the grid has not been revealed. In this article, the two-stage PV power system is developed with five different charging strategies. Moreover, comprehensive mathematical derivations of the charging power analysis will be revealed in this section. In the following, three different scenarios will be distinguished for each charging methods.

A. CC Charging

1) $I_{\rm PV}(D) = I_{\rm BAT,CC}$*:* First, Fig. 3(a) shows the case of the CC charging when the PV current $I_{\rm PV}(D)$ is equal to the battery current $I_{\rm BAT,CC}$. The inverter current $I_{\rm INV,CC}$ is set as zero as

$$I_{\rm INV,CC} = 0. \tag{1}$$

$I_{\rm PV}(D) > I_{\rm BAT,CC}$ or $I_{\rm PV}(D) < I_{\rm BAT,CC}$

The current mismatch scenarios of the CC charging are shown in Fig. 3(b) and (c). If the maximum PV current $I_{\rm MPP}(D)$ is larger/lower than $I_{\rm BAT,CC}$, the extra/inadequate current $\Delta I_{\rm CC}$ can be regulated by $I_{\rm INV,CC}$ as

$$I_{\rm INV,CC} = I_{\rm MPP}(D) - I_{\rm BAT,CC} = \Delta I_{\rm CC}. \tag{2}$$

It should be noticed that if $I_{\rm MPP}(D)$ is greater than $I_{\rm BAT,CC}$, $\Delta I_{\rm CC}$ will be a positive value while the inverter is operated with the inverter mode. On the other hand, if $I_{\rm MPP}(D)$ is lower than $I_{\rm BAT,CC}$, $\Delta I_{\rm CC}$ will be a negative value, whereas the inverter is operated with power factor corrector (PFC) mode.

Eventually, the power difference ΔP_{CC} will be equal to the inverter power $P_{\rm INV,CC}$ as the following equation shows:

$$\Delta P_{\rm CC} = P_{\rm PV} - P_{\rm BAT,CC} = P_{\rm INV,CC} \tag{3}$$

where $P_{\rm PV}$ is the PV power and $P_{\rm BAT,CC}$ is the battery power under the CC charging. With the expression of the battery voltage $V_{\rm BAT}$, (3) can be modified as

$$\Delta P_{\rm CC} = V_{\rm BAT} \times [I_{\rm MPP}(D) - I_{\rm BAT,CC}] = V_{\rm BAT} \times I_{\rm INV,CC}. \tag{4}$$

B. PRC Charging

Scenarios of the PRC charging are shown in Fig. 4. The battery charging power $P_{\rm BAT,PRC}$ can be written as

$$P_{\rm BAT,PRC} = V_{\rm BAT} \times \left(I_{\rm BAT,PRC} \times \frac{\Delta t}{T} \right) \tag{5}$$

where $I_{\rm BAT,PRC}$ is the peak battery current, Δt is the positive charging period, and T is the total charging period.

The inverter power $P_{\rm INV,PRC}$ should be the same as the power difference $\Delta P_{\rm PRC}$ as

$$\Delta P_{\rm PRC} = P_{\rm PV} - P_{\rm BAT,PRC} = P_{\rm INV,PRC}. \tag{6}$$

1) $I_{\rm PV}(D) = I_{\rm BAT,PRC}$*:* Fig. 4(a) shows the case of $I_{\rm MPP}(D)$ equal to $I_{\rm BAT,PRC}$. From Fig. 4 (a), it can be confirmed that the battery current waveform $I_{\rm BAT}$ and the inverter current waveform $I_{\rm INV}$ are complementary.

The inverter current under the PRC charging $I_{\rm INV,PRC}$ and the power difference $\Delta P_{\rm PRC}$ can be expressed as follows:

$$I_{\rm INV,PRC} = I_{\rm BAT,PRC} \left(1 - \frac{\Delta t}{T} \right) \tag{7}$$

$$\Delta P_{\rm PRC} = V_{\rm BAT} \times I_{\rm BAT,PRC} \left(1 - \frac{\Delta t}{T} \right). \tag{8}$$

2) $I_{\rm PV}(D) > I_{\rm BAT,PRC}$ *or* $I_{\rm PV}(D) < I_{\rm BAT,PRC}$*:* Fig. 4(b) shows the case of $I_{\rm MPP}(D)$ greater than $I_{\rm BAT,PRC}$, whereas Fig. 4(c) shows the case of $I_{\rm MPP}(D)$ lower than $I_{\rm BAT,PRC}$. The current difference $\Delta I_{\rm PRC}$ can be written as

$$\Delta I_{\rm PRC} = I_{\rm MPP}(D) - I_{\rm BAT,PRC}. \tag{9}$$

Different from (7), $\Delta I_{\rm PRC}$ should be included in $I_{\rm INV,PRC}$ to maintain the maximum PV power harvesting as

$$I_{\rm INV,PRC} = I_{\rm BAT,PRC} \left(1 - \frac{\Delta t}{T} \right) + \Delta I_{\rm PRC}. \tag{10}$$

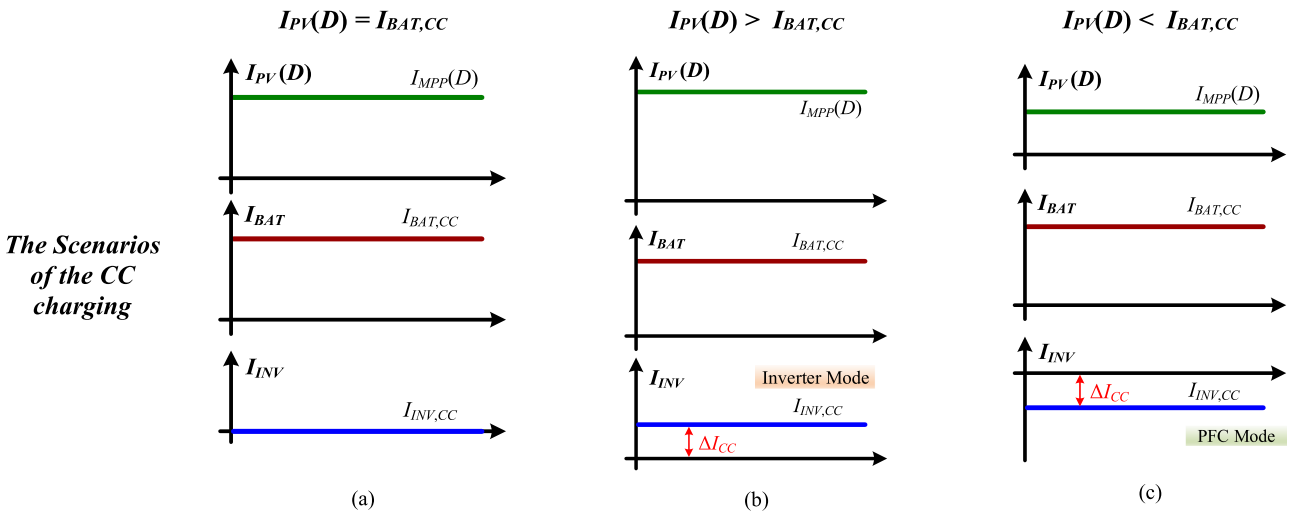

Fig. 3. Relations between $I_{\mathrm{PV}}(D)$, I_{BAT}, and I_{INV} under the CC charging. (a) $I_{\mathrm{PV}}(D) = I_{\mathrm{BAT,CC}}$. (b) $I_{\mathrm{PV}}(D) > I_{\mathrm{BAT,CC}}$. (c) $I_{\mathrm{PV}}(D) < I_{\mathrm{BAT,CC}}$.

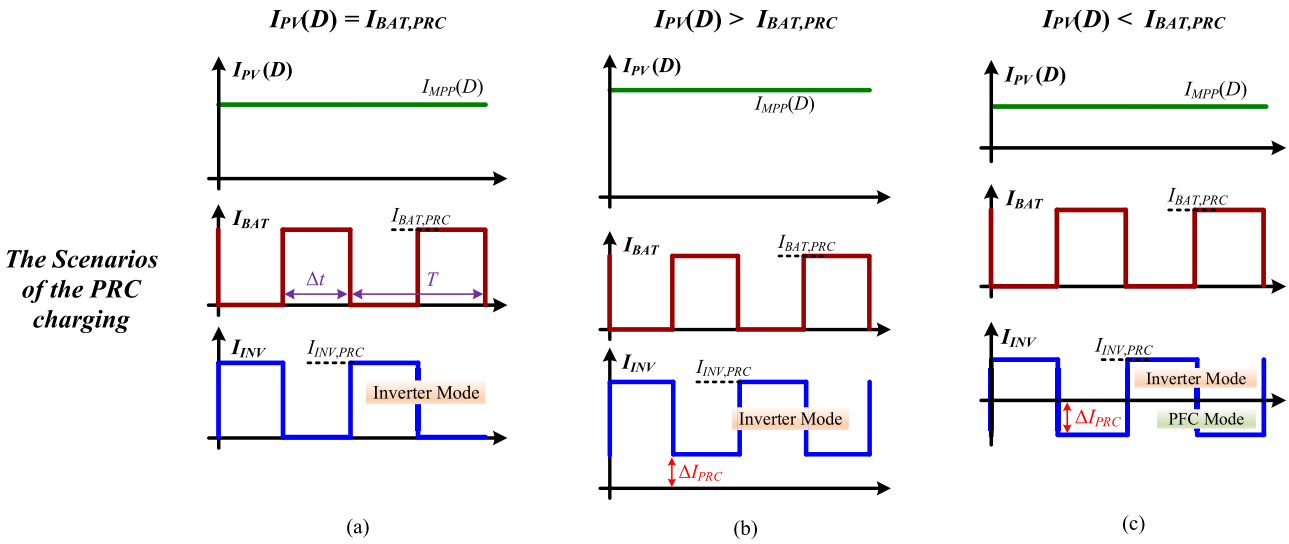

Fig. 4. Relations between $I_{\mathrm{PV}}(D)$, I_{BAT}, and I_{INV} under the PRC charging. (a) $I_{\mathrm{PV}}(D) = I_{\mathrm{BAT,PRC}}$. (b) $I_{\mathrm{PV}}(D) > I_{\mathrm{BAT,PRC}}$. (c) $I_{\mathrm{PV}}(D) < I_{\mathrm{BAT,PRC}}$.

Eventually, ΔP_{PRC} can be obtained as

$$\Delta P_{\mathrm{PRC}} = V_{\mathrm{BAT}} \times \left[I_{\mathrm{BAT,PRC}} \left(1 - \frac{\Delta t}{T} \right) + \Delta I_{\mathrm{PRC}} \right]. \tag{11}$$

It should be noticed that in Fig. 4(c), the rear-end inverter will switch between inverter mode and PFC mode.

C. SRC Charging

Scenarios of the SRC charging are shown in Fig. 5. First, the battery charging power $P_{\mathrm{BAT,SRC}}(t)$ can be defined as

$$P_{\mathrm{BAT,SRC}}(t) = V_{\mathrm{BAT}} \times \frac{1}{2} \left[I_{\mathrm{BAT,SRC}} \sin(\omega t) + I_{\mathrm{BAT,SRC}} \right] \tag{12}$$

where $I_{\mathrm{BAT,SRC}}$ is the peak battery current under the SRC charging.

1) $I_{\mathrm{PV}}(D) = I_{\mathrm{BAT,SRC}}$*:* First, if $I_{\mathrm{MPP}}(D)$ is equal to $I_{\mathrm{BAT,SRC}}$, as shown in Fig. 5(a), the average battery power $P_{\mathrm{BAT,SRC}}$ can be obtained as

$$P_{\mathrm{BAT,SRC}} = \frac{1}{2}(V_{\mathrm{BAT}} \times I_{\mathrm{BAT,SRC}}). \tag{13}$$

Besides, the charging power difference ΔP_{SRC} between P_{PV} and $P_{\mathrm{BAT,SRC}}$ can be calculated as

$$\Delta P_{\mathrm{SRC}} = P_{\mathrm{PV}} - P_{\mathrm{BAT,SRC}} = P_{\mathrm{INV,SRC}} = \frac{1}{2}(V_{\mathrm{BAT}} \times I_{\mathrm{BAT,SRC}}). \tag{14}$$

In order to achieve the maximum PV power output, the peak current command of the inverter $I_{\mathrm{INV,SRC}}$ should be equal to

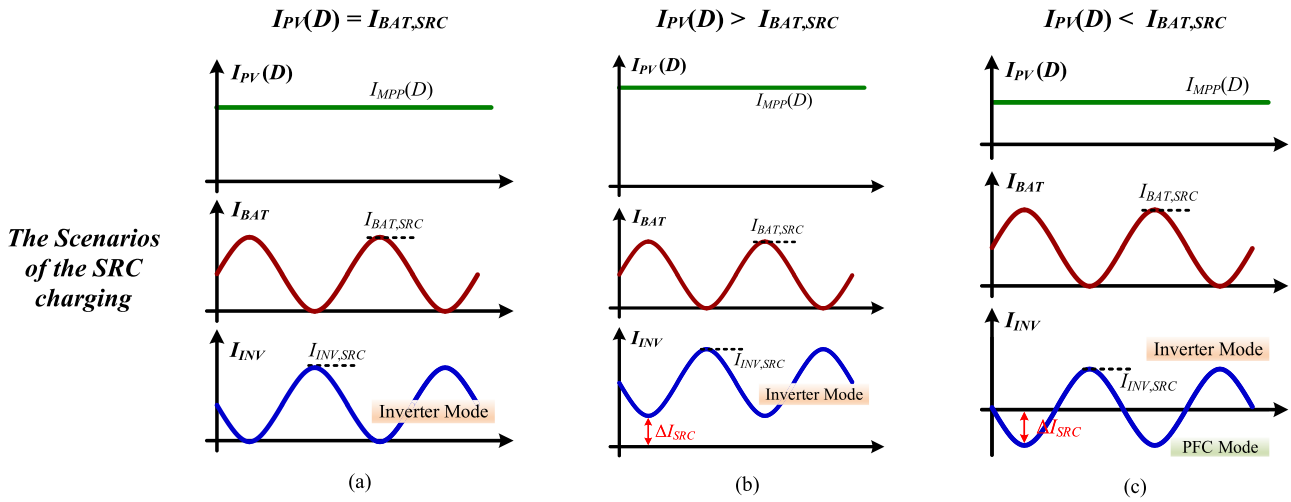

Fig. 5. Relations between $I_{\mathrm{PV}}(D)$, I_{BAT}, and I_{INV} under the SRC charging. (a) $I_{\mathrm{PV}}(D) = I_{\mathrm{BAT,SRC}}$. (b) $I_{\mathrm{PV}}(D) > I_{\mathrm{BAT,SRC}}$. (c) $I_{\mathrm{PV}}(D) < I_{\mathrm{BAT,SRC}}$.

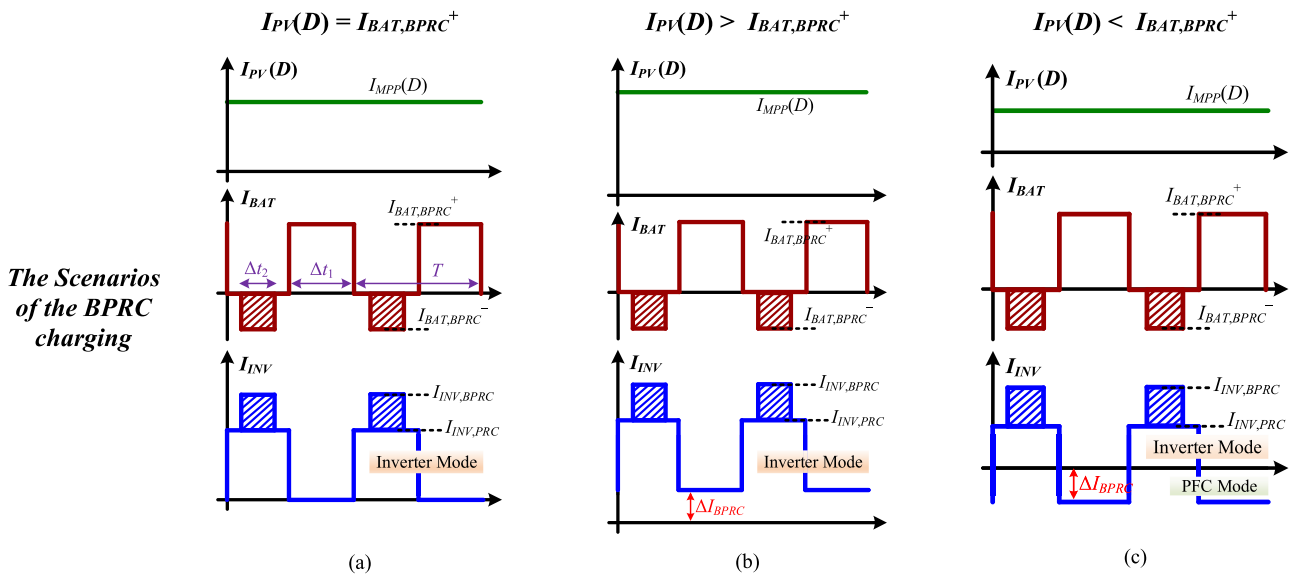

Fig. 6. Relations between $I_{\mathrm{PV}}(D)$, I_{BAT}, and I_{INV} under the BPRC charging. (a) $I_{\mathrm{PV}}(D) = I_{\mathrm{BAT,BPRC}}{}^{+}$. (b) $I_{\mathrm{PV}}(D) > I_{\mathrm{BAT,BPRC}}{}^{+}$. (c) $I_{\mathrm{PV}}(D) < I_{\mathrm{BAT,BPRC}}{}^{+}$.

$I_{\mathrm{BAT,SRC}}$ as

$$I_{\mathrm{INV,SRC}} = I_{\mathrm{BAT,SRC}}. \tag{15}$$

Besides, there should be a 180° out of phase shift between the battery current and inverter current. As a result, the inverter current command $I_{\mathrm{INV,SRC}}(t)$ can be derived as

$$I_{\mathrm{INV,SRC}}(t) = \frac{1}{2}\left[I_{\mathrm{BAT,SRC}}\sin(\omega t - \pi) + I_{\mathrm{BAT,SRC}}\right] \tag{16}$$

where ω is the angular frequency of the charging current.

2) $I_{\mathrm{PV}}(D) > I_{\mathrm{BAT,SRC}}$ or $I_{\mathrm{PV}}(D) < I_{\mathrm{BAT,SRC}}$: Fig. 5(b) and (c) shows cases of the PV current larger or lower than $I_{\mathrm{BAT,SRC}}$. The current difference ΔI_{SRC} can be written as

$$\Delta I_{\mathrm{SRC}} = I_{\mathrm{MPP}}(D) - I_{\mathrm{BAT,SRC}}. \tag{17}$$

Therefore, ΔI_{SRC} should be included in $I_{\mathrm{INV,SRC}}$, as

$$I_{\mathrm{INV,SRC}} = I_{\mathrm{BAT,SRC}} + \Delta I_{\mathrm{SRC}} \tag{18}$$

whereas ΔP_{SRC} can be modified as

$$\Delta P_{\mathrm{SRC}} = V_{\mathrm{BAT}} \times \left(\frac{1}{2} I_{\mathrm{BAT,SRC}} + \Delta I_{\mathrm{SRC}}\right). \tag{19}$$

It is worth mentioning that with the case of $I_{\mathrm{PV}}(D) < I_{\mathrm{BAT,SRC}}$, inverter will be operated in both inverter mode and PFC mode.

D. BPRC Charging

Fig. 6 shows scenarios of the BPRC charging strategy. Different from the PRC charging method, there will be both positive

and negative charging periods. However, due to the fact that the PV array cannot absorb energy, the discharging power should be transferred to the grid via the inverter, as the slanted line area shown in Fig. 6. In other words, the inverter current will be larger than the PV current during the battery discharging period. Then, the battery charging power $P_{\mathrm{BAT,BPRC}}$ can be defined as

$$P_{\mathrm{BAT,BPRC}} = V_{\mathrm{BAT}} \times \left[\left(I_{\mathrm{BAT,BPRC}}{}^{+} \times \frac{\Delta t_1}{T}\right) - \left(I_{\mathrm{BAT,BPRC}}{}^{-} \times \frac{\Delta t_2}{T}\right)\right] \tag{20}$$

whereas $I_{\mathrm{BAT,BPRC}}{}^{+}$ and $I_{\mathrm{BAT,BPRC}}{}^{-}$ are the peak positive charging current and peak negative charging current, respectively. Δt_1 and Δt_2 represent the positive charging period and negative charging period, respectively.

The charging power difference ΔP_{BPRC} between P_{PV} and $P_{\mathrm{BAT,BPRC}}$ can be calculated as

$$\Delta P_{\mathrm{BPRC}} = P_{\mathrm{PV}} - P_{\mathrm{BAT,BPRC}} = P_{\mathrm{INV,BPRC}} \tag{21}$$

where $P_{\mathrm{INV,BPRC}}$ is the inverter power under the BPRC charging.

1) $I_{\mathrm{PV}}(D) = I_{\mathrm{BAT,BPRC}}$: Fig. 6(a) shows the case of $I_{\mathrm{MPP}}(D)$ equal to $I_{\mathrm{BAT,BPRC}}{}^{+}$, as the following equation indicates:

$$I_{\mathrm{MPP}}(D) = I_{\mathrm{BAT,BPRC}}{}^{+}. \tag{22}$$

The inverter current under the PRC charging $I_{\mathrm{INV,BPRC}}$ and the power difference ΔP_{BPRC} can be expressed by the following equations:

$$I_{\mathrm{INV,BPRC}} = I_{\mathrm{BAT,BPRC}}{}^{+} \times \left(1 - \frac{\Delta t_1}{T}\right) + I_{\mathrm{BAT,BPRC}}{}^{-} \times \left(\frac{\Delta t_2}{T}\right) \tag{23}$$

$$\Delta P_{\mathrm{BPRC}} = V_{\mathrm{BAT}} \times \left[I_{\mathrm{BAT,BPRC}}{}^{+} \times \left(1 - \frac{\Delta t_1}{T}\right) + I_{\mathrm{BAT,BPRC}}{}^{-} \times \left(\frac{\Delta t_2}{T}\right)\right]. \tag{24}$$

2) $I_{\mathrm{PV}}(D) > I_{\mathrm{BAT,BPRC}}$ or $I_{\mathrm{PV}}(D) < I_{\mathrm{BAT,BPRC}}$: The current mismatch scenarios of the BPRC charging are shown in Fig. 6(b) and (c). The current difference ΔI_{BPRC} can be written as

$$\Delta I_{\mathrm{BPRC}} = I_{\mathrm{MPP}}(D) - I_{\mathrm{BAT,BPRC}}{}^{+}. \tag{25}$$

With the combination of (23) and (25), $I_{\mathrm{INV,BPRC}}$ can be modified as

$$I_{\mathrm{INV,BPRC}} = \left[I_{\mathrm{BAT,BPRC}}{}^{+} \times \left(1 - \frac{\Delta t_1}{T}\right) + I_{\mathrm{BAT,BPRC}}{}^{-} \times \left(\frac{\Delta t_2}{T}\right)\right] + \Delta I_{\mathrm{BPRC}}. \tag{26}$$

Consequently, ΔP_{BPRC} under the current mismatch scenario can be obtained as

$$\Delta P_{\mathrm{BPRC}} = V_{\mathrm{BAT}} \times \left\{\left[I_{\mathrm{BAT,BPRC}}{}^{+} \times \left(1 - \frac{\Delta t_1}{T}\right) + I_{\mathrm{BAT,BPRC}}{}^{-} \times \left(\frac{\Delta t_2}{T}\right)\right] + \Delta I_{\mathrm{BPRC}}\right\}. \tag{27}$$

E. BSRC Charging

The BSRC charging scenarios are shown in Fig. 7. First, the battery charging power $P_{\mathrm{BAT,BSRC}}$ can be expressed as

$$P_{\mathrm{BAT,BSRC}} = V_{\mathrm{BAT}} \times I_{\mathrm{BAT,BSRC,avg}} \tag{28}$$

where $I_{\mathrm{BAT,BSRC,avg}}$ is the average battery current. According to Fig. 7, $I_{\mathrm{BAT,BSRC,avg}}$ can be derived as (29) shown at the bottom of this page, $I_{\mathrm{BAT,BSRC}}{}^{+}$ and $I_{\mathrm{BAT,BSRC}}{}^{-}$ are the maximum positive and negative charging currents, respectively. x_1 and x_2 represent the starting and stopping angles of the discharging period, respectively. It should be noticed that x_1 should be within the range of π and $3\pi/2$. x_2 should be within the range of $3\pi/2$ and 2π as

$$\pi \le x_1 \le {}^{3\pi}/_{;2}{}^{3\pi}/_{2} \le x_2 \le 2\pi. \tag{30}$$

The charging power difference ΔP_{SPRC} between P_{PV} and $P_{\mathrm{BAT,SPRC}}$ can be defined as

$$\Delta P_{\mathrm{BSRC}} = P_{\mathrm{PV}} - P_{\mathrm{BAT,BSRC}} = P_{\mathrm{INV,BSRC}} \tag{31}$$

where $P_{\mathrm{INV,BSRC}}$ is the inverter power under the BSRC charging.

1) $I_{\mathrm{PV}}(D) = I_{\mathrm{BAT,BSRC}}$: Fig. 7(a) shows the case of $I_{\mathrm{MPP}}(D)$ equal to $I_{\mathrm{BAT,BSRC}}{}^{+}$ as

$$I_{\mathrm{MPP}}(D) = I_{\mathrm{BAT,BSRC}}{}^{+}. \tag{32}$$

According to Fig. 7(a), the inverter current command $I_{\mathrm{INV,SRC}}$ and $I_{\mathrm{INV,BSRC}}$ should be satisfied with the following equations to maintain the MPP operation of the PV array:

$$I_{\mathrm{INV,SRC}} = I_{\mathrm{BAT,BSRC}}{}^{+} \tag{33}$$

$$I_{\mathrm{INV,BSRC}} = I_{\mathrm{BAT,BSRC}}{}^{+} + \left|I_{\mathrm{BAT,BSRC}}{}^{-}\right|. \tag{34}$$

Eventually, the inverter current command under the BSRC, i.e., $I_{\mathrm{INV,BSRC}}(t)$, can be obtained as

$$I_{\mathrm{INV,BSRC}}(t) = I_{\mathrm{PV}}(D) - I_{\mathrm{BAT,BSRC}}(t). \tag{35}$$

$$I_{\mathrm{BAT,BSRC,avg}} = \frac{2\left(\int_0^{\pi/\omega} I_{\mathrm{BAT,BSRC}}{}^{+} \sin \omega t dt - \int_{x_1/\omega}^{x_2/\omega} I_{\mathrm{BAT,BSRC}}{}^{-} \sin \omega t dt\right)}{T_{\mathrm{charge}}} \tag{29}$$

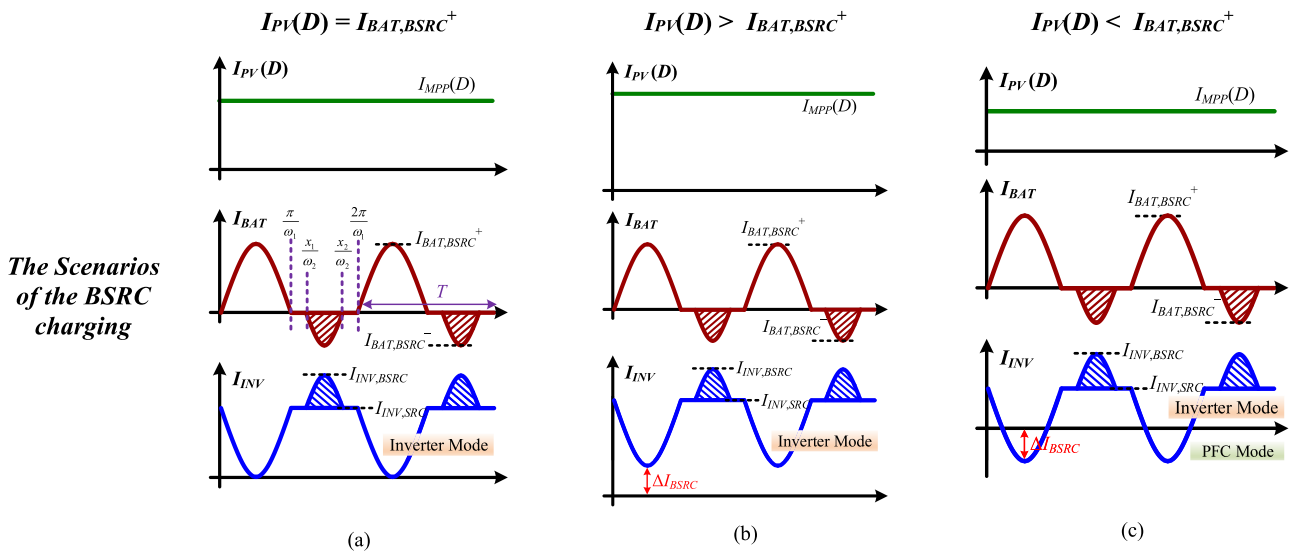

Fig. 7. Relations between $I_{\mathrm{PV}}(D)$, I_{BAT}, and I_{INV} under the BSRC charging. (a) $I_{\mathrm{PV}}(D) = I_{\mathrm{BAT,BSRC}}{}^{+}$. (b) $I_{\mathrm{PV}}(D) > I_{\mathrm{BAT,BSRC}}{}^{+}$. (c) $I_{\mathrm{PV}}(D) < I_{\mathrm{BAT,BSRC}}{}^{+}$.

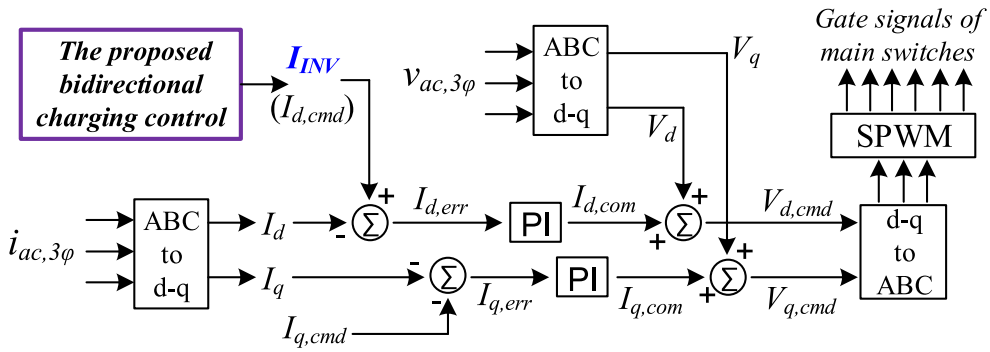

Fig. 8. Control block diagrams of the three-phase grid-tied inverter.

2) $I_{\mathrm{PV}}(D) > I_{\mathrm{BAT,BSRC}}$ or $I_{\mathrm{PV}}(D) < I_{\mathrm{BAT,BSRC}}$: Fig. 7(b) and (c) shows cases of the PV current is larger or lower than $I_{\mathrm{BAT,BSRC}}$. The current difference ΔI_{BSRC} can be written as

$$\Delta I_{\mathrm{BSRC}} = I_{\mathrm{MPP}}(D) - I_{\mathrm{BAT,BSRC}}. \tag{36}$$

Under the current mismatch scenario, ΔI_{BSRC} should be included in $I_{\mathrm{INV,BSRC}}(t)$ as

$$I_{\mathrm{INV,BSRC}}(t) = I_{\mathrm{PV}}(D) - I_{\mathrm{BAT,BSRC}}(t) + \Delta I_{\mathrm{BSRC}}. \tag{37}$$

Finally, ΔP_{BSRC} can be calculated as

$$\Delta P_{\mathrm{BSRC}} = V_{\mathrm{BAT}} \times (I_{\mathrm{BAT,BSRC,avg}} + \Delta I_{\mathrm{SRC}}). \tag{38}$$

From (4), (8), (11), (14), (19), (24), (27), (31), and (38), it can be confirmed that the adequate/inadequate energy will be regulated by the three-phase grid-tied inverter, whereas the PV current maintains a constant value. In other words, the maximum PV power utilization can be achieved by the proposed circuit and strategies.

It is worth mentioning that the timing signals of the converter are set as the same as the switching frequency 50 kHz. In addition, the front-end boost converter utilizes the traditional PI method to achieve the control strategy. For the rear-end inverter, the direct-quadrature (d-q) transformation is utilized [27] and [28]. With the d-q control, the three-phase ac voltage and current signals will be converted as dc components, as shown in Fig. 8. Therefore, only the dc components will be considered in the control loop, whereas the charging/discharging current can be directly regulated by the inverter input current I_{INV}.

IV. Experimental Verification

In this section, experimental results obtained from a 5 kVA PV power system and proposed charging strategies will be presented. First, the prototype circuit figure and key circuit parameters of the interleaved boost converter are shown in Fig. 9(a) and Table I, respectively. In should be mentioned that a PV simulator, Chroma 62150H, is adopted and connected to the input port of the boost converter. The input voltage and the input current are set as 250 V (V_{oc}), 200 V(V_{MPP}), 27.7 A (I_{sc}), and 25 A (I_{MPP}), respectively. The MOSFET, SPW47N60C3, is adopted as the main switches, whereas TLP350 is chosen as the gate driver. Besides, APT15D60BG is selected as the rectifier

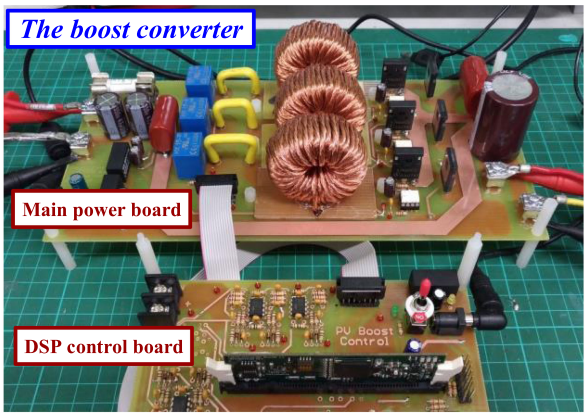

(a)

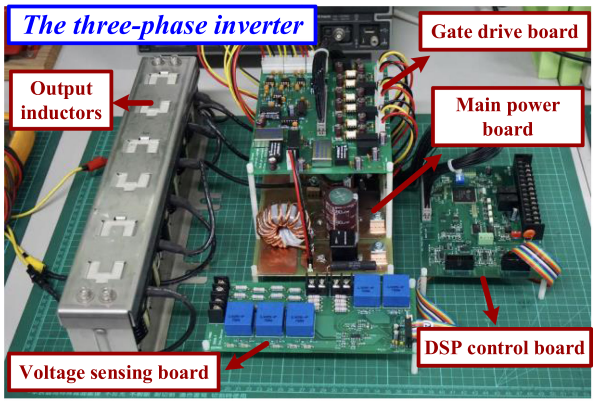

(b)

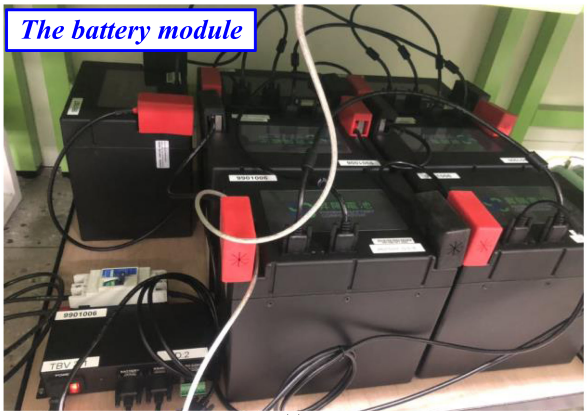

(c)

Fig. 9. Prototype hardware figures of the experimental setup. (a) Boost converter. (b) Three-phase inverter. (c) Battery module.

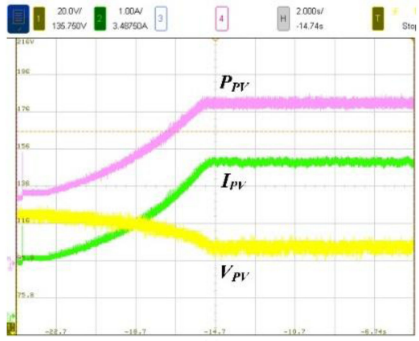

(a)

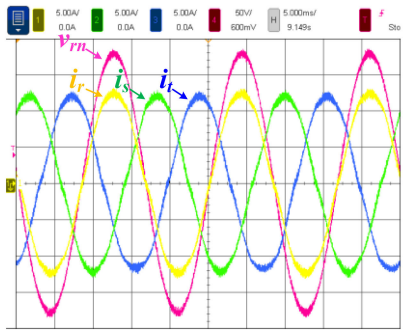

(b)

Fig. 10. Experimental waveform of (a) MPPT function. (b) Grid connected operation.

diodes of the boost converter. The DSP, TMS320F28335, is utilized as the circuit controller.

The prototype circuit figures of the three-phase grid-tied inverter are shown in Fig. 9(b). The main power board, the gate drive board, the voltage sensing board, the DSP control board, and output inductors are included in the hardware circuit. Main circuit specifications of the inverter are shown in Table II. According to the specifications of the battery, the input voltage and current of the inverter are determined as 320–397 V and 12.6 A, respectively. The output of the inverter is connected to the 220 $V_{\rm rms}$, 60 Hz three-phase power system. The rated output current is set as 13$A_{\rm rms}$. The silicon-carbide (SiC) MOSFETs, H1M065F020, are adopted in the main power stage, whereas TLP350 is selected as the gate drivers. The input inductance $L_{\rm in}$ and the input capacitance $C_{\rm in}$ are determined as 100 μH and 1.36 mF, respectively. The output inductance L_f and the output capacitance C_f are designed as 2 mH and 2.2 μF, respectively. The DSP, TMS320F28335 chip, is utilized as the system controller.

On the other hand, Fig. 9(c) and Table III show the photo and parameters of the battery module. The module consists of lithium iron phosphate battery. The capacity is 15AH, whereas the operational voltage is between 320 and 397 V. Besides, the C-rate can be calculated via the ratio of rated charging current and the battery capacity. According to the circuit specifications of this article, C-rate will be 0.84 C.

Experimental results of the MPPT function are shown in Fig. 10(a). It can be seen that $I_{\rm PV}$ and $P_{\rm PV}$ will be increased and reach the MPP by the P&O algorithm. Fig. 10(b) shows waveforms of the output voltage and currents of the inverter. The voltage of the r-phase $v_{\rm rn}$ is in phase with the r-phase current i_r. Therefore, the inverter injects active power to the grid.

Experimental results of the CC charging are shown in Fig. 11. First, Fig. 11(a) shows waveforms of $I_{\rm PV}(D)$, $I_{\rm BAT}$, and $I_{\rm INV}$, whereas Fig.11(b) shows $I_{\rm BAT,CC}$, $V_{\rm BAT}$, and the three-phase output currents i_r, i_s, and i_t under the CC charging. Because of

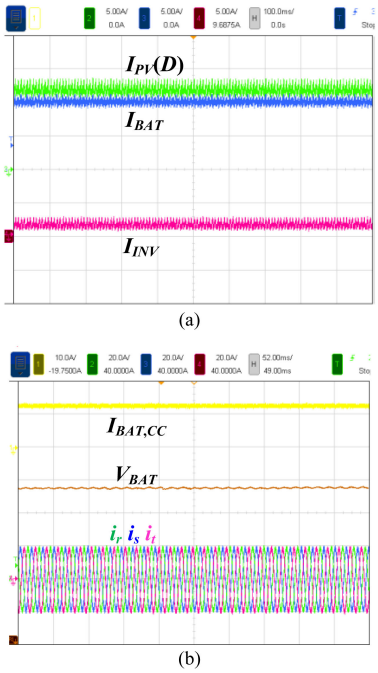

Fig. 11. Experimental results of the CC charging. (a) PV current, the battery current, and the inverter current. (b) Battery current, voltage, and output ac currents.

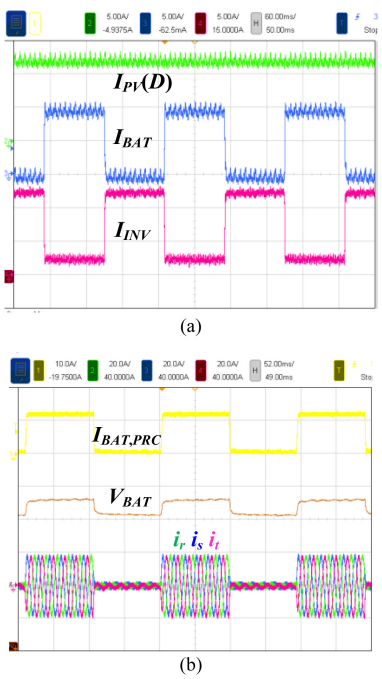

Fig. 12. Experimental results of the PRC charging. (a) PV current, the battery current, and the inverter current. (b) Battery current, voltage, and output ac currents.

the constant current charging characteristic, the battery current and voltage will be a constant value, whereas the three-phase output currents are balance.

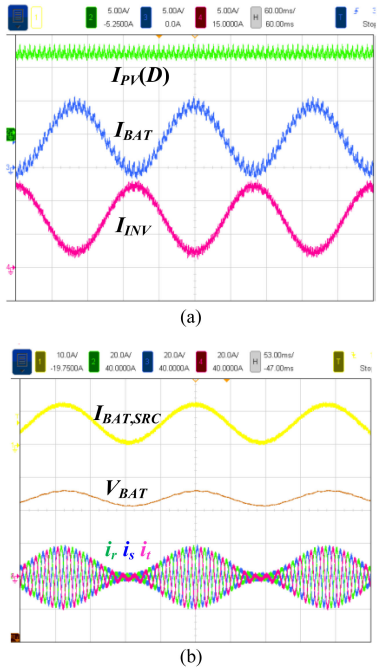

Fig. 13. Experimental results of the SRC charging. (a) PV current, the battery current, and the inverter current. (b) Battery current, voltage, and output ac currents.

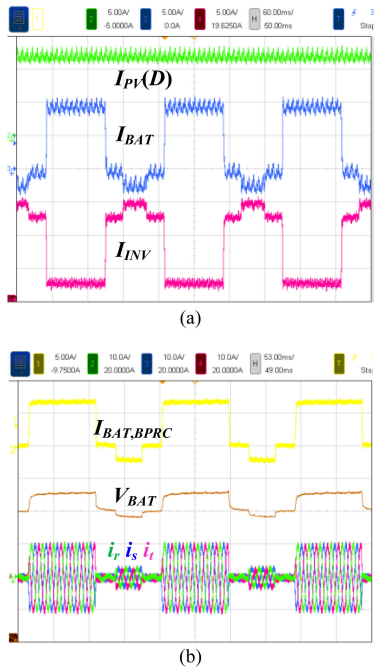

Fig. 14. Experimental results of the BPRC charging. (a) PV current, the battery current, and the inverter current. (b) Battery current, voltage, and output ac currents.

Waveforms of the PRC charging are shown in Fig. 12. Corresponding to the conceptual diagram shown in Fig. 4, the battery charging current will be controlled as a pulse form. I_{BAT} and I_{INV} will be complementary to remain the maximum

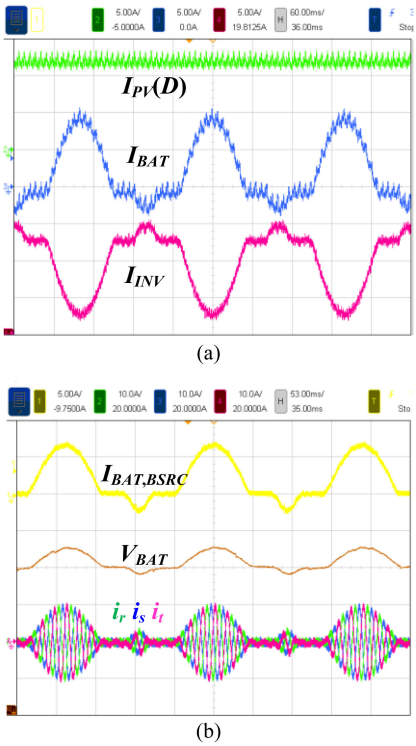

Fig. 15. Experimental results of the BSRC charging. (a) PV current, the battery current, and the inverter current. (b) Battery current, voltage, and output ac currents.

TABLE I
SPECIFICATIONS OF THE INTERLEAVED BOOST CONVERTER INVERTER

Parameters	Value
Rated power	5kW
Input voltage	250V(V_{oc}) / 200V(V_{mpp})
Input current	27.7A(I_{sc}) / 25A(I_{mpp})
Output voltage (Battery voltage)	320~397V
Rated output current	12.6A
Input inductance	760μH
Output capacitance	470uF/450V
Main switches	SPW47N60C3
Switching frequency	50kHz
Gate driver IC for the switches	TLP350
Output diodes	APT15D60BG
System controller	DSP TMS320F28335

PV current. Fig. 13 shows results of the SRC charging. According to the conceptual diagram shown in Fig. 5, the battery charging current will be controlled as a sinusoidal form. $I_{\rm BAT}$ and $I_{\rm INV}$ will be complementary to remain the maximum PV current.

Experimental results of the BPRC and BSRC charging are shown in Figs. 14 and 15, respectively. It can be seen that there will be positive current charging, negative current charging, and zero current charging period of the BPRC and BSRC charging.

TABLE II
SPECIFICATIONS OF THE THREE-PHASE GRID-TIED INVERTER

Parameters	Value
Rated power	5kVA
Input voltage (Battery voltage)	320~397V
Input rated current	12.6A
Grid voltages (Line-to-Line)	3-phase, 220V_{rms}, 60Hz
Rated output current	13A_{rms}
Main Switches	H1M065F020 (SiC MOSFET)
Switching frequency	50kHz
Gate driver IC for the switches	TLP350
Input inductance, L_{in}	100μH
Input capacitance, C_{in}	1.36mF
Output inductance, L_f	2mH
Output capacitance, C_f	2.2μF
System controller	DSP TMS320F28335

TABLE III
SPECIFICATIONS OF THE BATTERY MODULE

Parameters	Value
Battery type	Lithium iron phosphate battery
Battery Capacity	15AH
Rated voltage	397V
Cut-off voltage	320V
C-Rate	0.84C

In addition, the complementarity of $I_{\rm BAT}$ and $I_{\rm INV}$ ensure the maximum PV power harvesting.

V. CONCLUSION

This article proposes bidirectional power flow control and hybrid charging strategies for the three-phase PV power and energy storage systems. First, five charging methods, including the CC, PRC, SRC, BPRC, and BSRC charging, are considered and adopted for the battery. On the other hand, a three-phase grid-tied inverter integrated with proposed bidirectional power flow control strategies is adopted for the PV power system. With these strategies, the power flow between the PV, the battery, and the inverter can be dynamically regulated according to different charging scenarios. As a result, there is no need to abandon the MPPT function, whereas the maximum PV power utilization can be achieved. The proposed strategies can be realized by DSPs without including additional circuits and components. Detailed analysis and mathematical derivations are also revealed. Finally, experimental results obtained from a 5-kW prototype verify the performance and feasibility of the proposed circuit and control strategies.

ACKNOWLEDGMENT

The authors would like to thank the invaluable support with the experimental setup from the Electric Energy Processing

Laboratory (EEPro), Department of Electrical Engineering, National Taiwan University.

REFERENCES

[1] S. Hasanpour, Y. P. Siwakoti, A. Mostaan, and F. Blaabjerg, "New semi-quadratic high step-up DC/DC converter for renewable energy applications," *IEEE Trans. Power Electron.*, vol. 36, no. 1, pp. 433–446, Jan. 2021.

[2] S. Golestan, J. M. Guerrero, J. C. Vasquez, A. M. Abusorrah, and Y. Al-Turki, "Harmonic linearization and investigation of three-phase parallel-structured signal decomposition algorithms in grid-connected applications," *IEEE Trans. Power Electron.*, vol. 36, no. 4, pp. 4198–4213, Apr. 2021.

[3] Z. Tang, Y. Yang, and F. Blaabjerg, "An interlinking converter for renewable energy integration into hybrid grids," *IEEE Trans. Power Electron.*, vol. 36, no. 3, pp. 2499–2504, Mar. 2021.

[4] M. A. Ghasemi, H. M. Foroushani, and F. Blaabjerg, "Marginal power-based maximum power point tracking control of photovoltaic system under partially shaded condition," *IEEE Trans. Power Electron.*, vol. 35, no. 6, pp. 5860–5872, Jun. 2020.

[5] Z. Huang, Q. Li, and F. C. Lee, "Critical-conduction-mode-based soft-switching modulation for three-phase PV inverters with reactive power transfer capability," *IEEE Trans. Power Electron.*, vol. 35, no. 6, pp. 5702–5713, Jun. 2020.

[6] C. Tang, Y. Chen, and Y. Chen, "PV power system with multi-mode operation and low-voltage ride-through capability," *IEEE Trans. Ind. Electron.*, vol. 62, no. 12, pp. 7524–7533, Dec. 2015.

[7] S. Selvakumar, M. Madhusmita, C. Koodalsamy, S. P. Simon, and Y. R. Sood, "High-speed maximum power point tracking module for PV systems," *IEEE Trans. Ind. Electron.*, vol. 66, no. 2, pp. 1119–1129, Feb. 2019.

[8] H. Li, D. Yang, W. Su, J. Lü, and X. Yu, "An overall distribution particle swarm optimization MPPT algorithm for photovoltaic system under partial shading," *IEEE Trans. Ind. Electron.*, vol. 66, no. 1, pp. 265–275, Jan. 2019.

[9] N. Kumar, B. Singh, B. K. Panigrahi, and L. Xu, "Leaky-least-logarithmic-absolute-difference-based control algorithm and learning-based InC MPPT technique for grid-integrated PV system," *IEEE Trans. Ind. Electron.*, vol. 66, no. 11, pp. 9003–9012, Nov. 2019.

[10] A. B. Khan and W. Choi, "Optimal charge pattern for the high-performance multistage constant current charge method for the li-ion batteries," *IEEE Trans. Energy Convers.*, vol. 33, no. 3, pp. 1132–1140, Sep. 2018.

[11] M. A. Hannan, M. M. Hoque, S. E. Peng, and M. N. Uddin, "Lithium-ion battery charge equalization algorithm for electric vehicle applications," *IEEE Trans. Ind. Appl.*, vol. 53, no. 3, pp. 2541–2549, May/Jun. 2017.

[12] C. Zhang, K. Li, J. Deng, and S. Song, "Improved realtime state-of-charge estimation of $LiFePO_4$ battery based on a novel thermoelectric model," *IEEE Trans. Ind. Electron.*, vol. 64, no. 1, pp. 654–663, Jan. 2017.

[13] W. Han, C. Zou, C. Zhou, and L. Zhang, "Estimation of cell SOC evolution and system performance in module-based battery charge equalization systems," *IEEE Trans. Smart Grid*, vol. 10, no. 5, pp. 4717–4728, Sep. 2019.

[14] Y. Wang, Y. Li, L. Jiang, Y. Huang, and Y. Cao, "PSO-based optimization for constant-current charging pattern for li-ion battery," *Chin. J. Electr. Eng.*, vol. 5, no. 2, pp. 72–78, Jun. 2019.

[15] V. Vu, D. Tran, and W. Choi, "Implementation of the constant current and constant voltage charge of inductive power transfer systems with the double-sided LCC compensation topology for electric vehicle battery charge applications," *IEEE Trans. Power Electron.*, vol. 33, no. 9, pp. 7398–7410, Sep. 2018.

[16] J. Ahn and B. K. Lee, "High-efficiency adaptive-current charging strategy for electric vehicles considering variation of internal resistance of lithium-ion battery," *IEEE Trans. Power Electron.*, vol. 34, no. 4, pp. 3041–3052, Apr. 2019.

[17] K. Noh, M. Zhang, and E. Sánchez-Sinencio, "A unified amplifierbased CC-CV linear charger for energy-constrained low-power applications," *IEEE Trans. Circuits Syst. II, Express Briefs*, vol. 66, no. 3, pp. 377–381, Mar. 2019.

[18] L. Chen, J. Chen, C. Ho, S. Wu, and D. Shieh, "Improvement of Li-ion battery discharging performance by pulse and sinusoidal current strategies," *IEEE Trans. Ind. Electron.*, vol. 60, no. 12, pp. 5620–5628, Dec. 2013.

[19] H. Chen, H. Chou, S. Wu, H. Chen, and L. Chen, "Reflex^{TM} waveform discussed by AC impedance impact on lithium-ion battery charging effects," in *Proc. IEEE 9th Conf. Ind. Electron. Appl.*, 2014, pp. 146–150.

[20] C. Lai, J. Teh, Y. Cheng, and Y. Li, "A reflex-charging based bidirectional DC charger for light electric vehicle and DC-microgrids," in *Proc. IEEE 10th TENCON*, 2017, pp. 280–284.

[21] Y. Zhao, R. Fu, and S. Choe, "Modeling of SEI formation based on a electrochemical reduced order model for Li(MnNiCo)O2/Carbon polymer battery," in *Proc. IEEE Veh. Power Propulsion Conf.*, 2015, pp. 1–4.

[22] P.-T. Chen, F.-H. Yang, T. Sangeetha, H.-M. Gao, and K. D. Huang, "Moderate energy for charging Li-ion batteries determined by first-principles calculations," *Batteries Supercaps*, vol. 1, pp. 209–214, 2018.

[23] P.-T. Chen *et al.*, "Reviving aged lithium-ion batteries and prolonging their cycle life by sinusoidal waveform charging strategy," *Batteries Supercaps*, vol. 2, pp. 673–677, 2019.

[24] C. Tang and T. Hsieh, "Dynamic energy regulation strategies with multi charging methods for photovoltaic chargers," *IEEE Trans. Sustain. Energy*, vol. 11, no. 3, pp. 1985–1994, Jul. 2020.

[25] C.-Y. Tang, P.-T. Chen, and J.-H. Jheng, "Bidirectional power flow control integrated with pulse and sinusoidal-ripple-current charging strategies for three-phase grid-tied converters," *IEEE Access*, vol. 9, pp. 42151–42160, 2021.

[26] C. Tang, P. Chen, and Y. Chen, "A three-phase battery charger with constant current and pulse-ripple-current charging capability," in *Proc. IEEE 4th Int. Future Energy Electron. Conf.*, 2019, pp. 1–5.

[27] S. Gao, H. Zhao, Y. Gui, D. Zhou, and F. Blaabjerg, "An improved direct power control for doubly fed induction generator," *IEEE Trans. Power Electron.*, vol. 36, no. 4, pp. 4672–4685, Apr. 2021.

[28] C. Tang, L. Kao, Y. Chen, and S. Ou, "Dynamic power decoupling strategy for three-phase PV power systems under unbalanced grid voltages," *IEEE Trans. Sustain. Energy*, vol. 10, no. 2, pp. 540–548, Apr. 2019.

Cheng-Yu Tang (Member, IEEE) received the B.S degree in electrical engineering from the National Kaohsiung University of Applied Sciences, Kaohsiung, Taiwan, in 2010, the M.S. degree in electrical engineering from the National Taipei University of Technology, Taipei, Taiwan, in 2012, and the Ph.D. degree in electrical engineering from the Department of Electrical Engineering, National Taiwan University, Taipei, Taiwan, in 2016.

He is currently an Associate Professor with the Department of Electrical Engineering, National Taipei University of Technology, Taipei, Taiwan. His research interests include switching power supplies, renewable energy systems, and power flow control.

Pon-Tzu Chen received the B.S. degree in electrical engineering from Feng-Chia University, Taichung, Taiwan, in 2017, and the M.S. degree in electrical engineering from the National Taiwan University, Taipei, Taiwan, in 2020.

She is currently the Application Engineer with Silergy Technology Inc., Kaohsiung, Taiwan. Her current research interests include the power electronics and bidirectional three-phase charger.

Jia-He Jheng received the B.S degree in electrical engineering from the National Ilan University, Ilan, Taiwan, in 2019. He is currently working toward the M.S. degree in electrical engineering with the Department of Electrical Engineering, National Taipei University of Technology, Taipei, Taiwan.

His research interests include applications of switching power supplies, renewable energy systems, and the power flow control.